AGU PUBLICATIONS

JGR

Journal of Geophysical Research: Atmospheres

RESEARCH ARTICLE
10.1002/2016JD025094

Key Points:
- Separate soil columns for PFTs allow the isolation of the effects of land cover on local climate from other forcings and feedbacks in GCMs
- The implicit transfer of energy through a shared soil column among PFTs complicates the analysis of subgrid data from land models
- The individual columns produce a subgrid air temperature response to deforestation that agrees well with previous observations

Supporting Information:
- Supporting Information S1

Correspondence to:
N. M. Schultz,
natalie.schultz@yale.edu

Citation:
Schultz, N. M., X. Lee, P. J. Lawrence, D. M. Lawrence, and L. Zhao (2016), Assessing the use of subgrid land model output to study impacts of land cover change, *J. Geophys. Res. Atmos.*, *121*, doi:10.1002/2016JD025094.

Received 14 MAR 2016
Accepted 7 MAY 2016
Accepted article online 12 MAY 2016

Assessing the use of subgrid land model output to study impacts of land cover change

Natalie M. Schultz[1], Xuhui Lee[1,2], Peter J. Lawrence[3], David M. Lawrence[3], and Lei Zhao[4]

[1]School of Forestry and Environmental Studies, Yale University, New Haven, Connecticut, USA, [2]Yale-NUIST Center on Atmospheric Environment, Nanjing University of Information Science and Technology, Nanjing, China, [3]National Center for Atmospheric Research, Boulder, Colorado, USA, [4]Program in Science, Technology and Environmental Policy (STEP), Woodrow Wilson School of Public and International Affairs, Princeton University, Princeton, New Jersey, USA

Abstract Subgrid information from land models has the potential to be a powerful tool for investigating land-atmosphere interactions, but relatively few studies have attempted to exploit subgrid output. In this study, we modify the configuration of the Community Land Model version CLM4.5 so that each plant functional type (PFT) is assigned its own soil column. We compare subgrid and grid cell-averaged air temperature and surface energy fluxes from this modified case (PFTCOL) to a case with the default configuration—a shared soil column for all PFTs (CTRL)—and examine the difference in simulated surface air temperature between grass and tree PFTs within the same grid cells (ΔT_{GT}). The magnitude and spatial patterns of ΔT_{GT} from PFTCOL agree more closely with observations, ranging from −1.5 K in boreal regions to +0.6 K in the tropics. We find that the column configuration has a large effect on PFT-level energy fluxes. In the CTRL configuration, the PFT-level annual mean ground heat flux (G) differs substantially from zero. For example, at a typical tropical grid cell, the annual G is 31.8 W m^{-2} for the tree PFTs and −14.7 W m^{-2} for grass PFTs. In PFTCOL, G is always close to zero. These results suggest that care must be taken when assessing local land cover change impacts with subgrid information. For models with PFTs on separate columns, it may be possible to isolate the differences in land surface fluxes between vegetation types that would be associated with land cover change from other climate forcings and feedbacks in climate model simulations.

1. Introduction

Land cover change influences global and local climate by altering terrestrial carbon storage and atmospheric CO_2 concentrations (biogeochemical effect) and by modifying surface radiation and turbulent fluxes (biophysical effect) [e.g., *Bala et al.,* 2007; *Bonan*, 2008; *Ciais et al.,* 2013; *Mahmood et al.,* 2014]. The biophysical effects of land cover change, which include changes to surface fluxes of radiation, heat, moisture, and momentum [*Pielke et al.,* 1998], are especially important for regional and local surface climate [*de Noblet-Ducoudré et al.,* 2012; *Lawrence and Chase*, 2010]. The biophysical effects of land cover change can be summarized by changes in (1) surface albedo, (2) evapotranspiration, and (3) roughness length and turbulent exchange, with their contribution on local climate quantified by changes in surface air temperature [*Bonan*, 2008; *Mahmood et al.,* 2014]. The relative importance of these three competing effects varies geographically and may amplify or dampen changes in surface climate caused by rising atmospheric greenhouse gas concentrations.

Understanding and quantifying the biophysical effects of land cover change on local climate are important for distinguishing between different anthropogenic forcings, but this understanding is hindered by a number of methodological challenges. Observational and modeling studies tend to agree on the latitudinal pattern of the temperature response to deforestation, with cooling in high latitudes and warming in low latitudes [e.g., *Davin and de Noblet-Ducoudré*, 2010; *Lawrence and Chase*, 2010; *Lee et al.,* 2011; *Zhang et al.,* 2014]. However, while observational methods have helped answer some major questions, they are limited by relatively short and sporadic measurement periods. Data that can be used to robustly and directly quantify the relative impact of the various biophysical processes on temperature differences for different land cover types are sparse and frequently suffer from some limitations such as differing underlying atmospheric conditions [*Lee et al.,* 2011; *Pielke et al.,* 2011]. Utilizing global climate models (GCMs) to assess the impact of biophysical land cover changes poses its own set of challenges [*de Noblet-Ducoudré et al.,* 2012; *Pielke et al.,* 2011; *Pitman et al.,* 2009]. Most modeling studies use two sets of simulations to evaluate the biophysical effects of historic land cover change: one with preindustrial or potential vegetation land cover and the other with present-day land cover, isolating the biophysical effects of land cover by prescribing the same atmospheric concentrations of

CO_2 and other greenhouse gases with both sets of land cover conditions [e.g., *Lawrence and Chase*, 2010]. Other modeling studies have taken it a step farther and applied the so-called "scorched Earth" strategy [*Pielke et al.,* 2011] in which the biophysical effects from a completely deforested world are compared to a fully forested world [e.g., *Davin and de Noblet-Ducoudré*, 2010]. Identifying and evaluating the biophysical effects of land cover change as the difference between two modeling scenarios is complicated by the need to properly establish that modeled land cover change climate signals cannot be simply explained as unforced model variability or nonlocal effects of land cover change such as changes to atmospheric or ocean circulation [*Pielke et al.*, 2011; *Pitman et al.*, 2009]. In addition, differences in the parameterization of vegetation types and the implementation of land cover change among land models lead to inconsistencies in biophysical effects of historical land cover change between different GCMs [*de Noblet-Ducoudré et al.,* 2012; *Pitman et al.,* 2009].

While some modeling studies have implemented land cover change as a fractional change in the distribution of vegetation within a grid cell, analyses have still focused on the grid cell-averaged difference of surface variables such as air temperature and energy fluxes [*Lawrence and Chase*, 2010; *Pitman et al.,* 2009]. Many terrestrial models represent land cover heterogeneity within a grid cell as a mosaic of subgrid tiles with distinct physical, biogeochemical, and ecological properties. However, few studies have attempted to utilize the subgrid information to assess the biophysical effects of land cover change. A notable exception is the recent study by *Malyshev et al.* [2015]. Their treatment of land cover tiles in the land component, LM3.0, of the Geophysical Fluid Dynamics Laboratory (GFDL) Earth System Model, ESM2Mb, captures the above- and below-ground heterogeneities of land cover types within a grid cell, allowing for the comparison of the response of different land cover types to the same atmospheric forcing.

Representing subgrid land surface heterogeneity in global climate models has long been a challenging problem. In early versions of GCMs, land surface parameters were often set to those of the dominant vegetation type within a grid cell [*Arain et al.,* 1999]. However, recognizing that significant spatial variability in vegetation and other features exist within the spatial area of a single model grid cell, new strategies for representing subgrid land surface heterogeneity were developed. At the two extremes are the "mixture" and "mosaic" approaches. At one end of the spectrum is the "mixture" strategy, which assumes that the different vegetation types are homogenously mixed within a grid cell, and the average of the structural, ecological, and physiological attributes of the vegetation types within the grid cell is used for surface calculations. The atmospheric model then interacts with the surface fluxes computed from this vegetation composite [*Koster and Suarez*, 1992]. At the other end of the spectrum is the "mosaic" strategy, which represents different land cover types as geographically distinct regions, each interacting with the atmospheric model separately, with no interaction between the tiles. In a full mosaic approach, in addition to surface energy and water fluxes computed for each individual tile, soil temperature, moisture, and snow cover evolve independently for each vegetation tile [*Koster and Suarez*, 1992; *Li and Arora*, 2012; *Molod*, 2002].

Many current versions of GCMs use land surface heterogeneity strategies that lie between the mixture and the "full mosaic" approaches described above. The land surface representation within the Community Land Model (CLM), the land component of the Community Earth System Model (CESM), consists of up to 15 plant functional types (PFTs) within the vegetated "land unit" of the grid cell [*Oleson et al.,* 2013]. Biogeochemical and biophysical fluxes are computed at the PFT level and then aggregated (area weighted) to the column level, in CLM nomenclature. While the PFTs within CLM can be thought of as a tile or mosaic surface configuration, all PFTs within the naturally vegetated land unit of the grid cell share a single soil column, with shared soil (temperature and moisture) and snow properties (see section 2 for more details). A single atmospheric forcing is applied to all PFT tiles within a grid cell. This type of land surface representation is consistent, at least broadly, with many other models in phase 5 of the Coupled Model Intercomparison Project (CMIP5) [*Malyshev et al.,* 2015].

Subgrid information from climate models can be a powerful tool for investigating land-atmosphere interactions, yet PFT-level output from land models has been underutilized in land cover change studies in favor of grid cell-averaged output. In contrast, subgrid information from nonvegetated land surface tiles has been used in CLM modeling experiments. For example, urban tiles within a grid cell have been used to investigate the contribution of local background climate to urban heat islands [*Zhao et al.,* 2014], and the subgrid lake model has been used to study lake-atmosphere interactions and the modulating effects of lakes on regional climate [*Deng et al.,* 2013; *Subin et al.,* 2012]. Perhaps part of the reason that individual PFT tiles have not been

frequently used in GCM experiments is because of the common characteristic of a shared soil column, which does not allow for the complete separation of each PFT from the others.

It is debatable whether the mixture or full mosaic strategy is a more "realistic" representation of the natural landscape in a model grid cell. The mixture approach is perhaps more appropriate for savanna-like landscapes where trees and grasses are interspersed and competing for water and nutrients. The mosaic approach may be more appropriate for regions with distinct areas of different land cover types. A potential advantage of the full mosaic approach is that it may be able to more clearly isolate the role and response of different vegetation types. Using CESM as an example, since the same atmospheric forcing is applied to PFT tiles, the differing responses of each vegetation type to the same atmospheric forcing can be examined. By directly comparing the response of one land cover type to another within the same grid cell, the complicating factors that arise from multiple simulations, unforced variability or nonlocal effects of land cover change, are no longer relevant. Additionally, analysis of subgrid information may be useful in future climate projection simulations to help understand how local biophysical effects of land cover change compared to other large-scale forcings, like a doubling of CO_2 for example.

In this study, we modify the subgrid PFT configuration of CLM4.5 so that it may be used to isolate the effects of land cover and land cover change on local climate. We compare the default (multiple vegetation types on a shared soil column) version to a modified version in which each PFT is given an individual soil column. Our specific objectives are to: (1) examine the effect of a shared soil column versus individual soil column configuration on subgrid (PFT level) and grid cell-averaged output of surface air temperature and energy fluxes, and (2) perform preliminary evaluation of the individual PFT column configuration to determine whether it may provide an advantage over the shared column configuration in land cover change experiments.

2. Methods

2.1. Model Description

The Community Land Model (CLM) [*Lawrence et al.,* 2011; *Oleson et al.,* 2013] is the land component of the Community Earth System Model (CESM) [*Hurrell et al.,* 2013]. In CLM4.5, the latest version of CLM, the land surface is represented as a nested hierarchy of subgrid levels. At the broadest level, the land unit, each grid cell may be divided into fractions of natural vegetation, lakes, urban areas, glaciers, and crops. The second subgrid level for the vegetated land unit is the column, which captures variations in soil and snow variables within the land unit. The soil profile in the vegetated land unit in CLM4.5 is represented as 15 discrete layers (to a depth of 35 m, with more soil layers near the surface). Hydrology calculations are done for just the top 10 layers (from the surface to the depth of 2.9 m), while soil temperature is calculated for all 15 layers. Up to five additional layers may be added for snow, depending on snow depth. The vegetated land unit is assigned a single column, with fractional areas of all the relevant plant functional types (PFTs) for that grid cell sharing the column.

The PFT level, or third subgrid level, specifies the differences in the biophysical and biogeochemical processes across different vegetation types. In addition to bare ground, the vegetated land unit may be composed of up to 15 different PFTs. PFTs differ in their optical properties, as well as their water uptake, aerodynamic, and photosynthetic parameters. The PFT parameterizations control the surface energy and biogeochemical fluxes from the vegetated surface. Fluxes from the land surface are computed at the PFT level and then area weighted to the column, land unit, and then grid cell level before being passed to the atmosphere model. The same atmospheric forcing is used to force all PFTs within the grid cell.

2.2. Experimental Setup

Two CLM4.5 simulations were run to investigate the effects of a shared soil column versus individual PFT columns on both the PFT-level and grid cell-level outputs of surface state variables and fluxes. The first simulation (CTRL) was run using the default configuration of CLM4.5, where all PFTs within a grid cell shared a single soil column. The second simulation (PFTCOL) was run using a modified version of CLM4.5, where each PFT within the vegetated land unit was assigned to its own soil column (Figure 1). Both the CTRL and PFTCOL simulations were run with present-day land cover conditions, with vegetation phenology (leaf area index (LAI) and stem area index (SAI)) prescribed by satellite observations [*Lawrence and Chase*, 2007; *Myneni et al.,* 2002]. In both simulations, CLM4.5 was run offline, driven with 1991–2010 CRUNCEP atmospheric

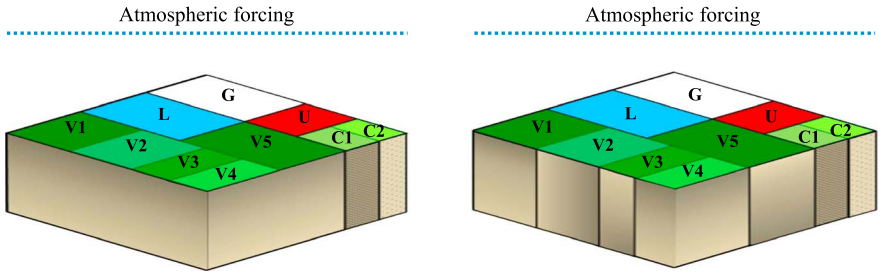

Figure 1. Schematic diagram illustrating the above- and below-ground configurations of CLM4.5 in the (a) CTRL and (b) PFTCOL simulations. A hypothetical grid cell may contain multiple land units (G—glacier, L—lake, U—urban, V—vegetated, and C—crop). By default, natural PFTs share a single soil column (CTRL). In the modified configuration (PFTCOL), each natural PFT is assigned its own soil column. For both the CTRL and PFTCOL cases, atmospheric inputs (incoming solar and longwave radiation, temperature, specific humidity, wind, pressure, and precipitation) are the same for all tiles within the grid cell.

forcing data [*Viovy*, 2011]. Each case was run for 81 years, with the first 60 years devoted to spin-up of soil temperature and moisture. PFT-level output and grid cell averages were archived for all surface and below-ground state and flux variables at monthly intervals for the first 80 years and then at hourly intervals for the final year.

2.3. Comparative Analysis

We conducted a comparative analysis of air temperature and surface energy fluxes at both the PFT-level and grid cell-level between the PFTCOL and CTRL simulations. The purpose of this comparison was to quantify the effect of the column configuration on subgrid and grid cell-averaged surface climate variables. For the PFT-level comparisons, we area weighted the grass and tree PFTs within each grid cell into a single value for each of these respective land cover categories. Although some grid cells contained other PFTs, including bare soil and shrubs, our analysis focuses on tree and grass PFTs for two reasons. First, we were interested in comparing how PFTs from distinct land cover classes responded to the change in column configuration. Second, these two broad classes had the widest spatial distribution across the globe (i.e., there were more grid cells that contained both tree and grass PFTs). It should be noted that the grid cell-averaged values do contain all PFTs within each grid cell, because in addition to examining PFT-level differences, we wanted to investigate whether this new configuration could affect atmospheric processes when coupled to the atmosphere model. We present the comparison as the difference (Δ) in surface climate variables between the PFTCOL and CTRL simulations (PFTCOL − CTRL). For example, ΔT_a is the difference in air temperature between the PFTCOL and CTRL cases. We also examined the difference in each term in the surface energy balance equation (equation (1)).

$$R_{\text{net}} = K\downarrow - K\uparrow + L\downarrow - L\uparrow = H + \lambda E + G \tag{1}$$

Incoming shortwave ($K\downarrow$) and longwave ($L\downarrow$) were prescribed by the atmospheric forcing data and therefore did not vary between the PFTCOL and CTRL cases. We compared the differences in reflected shortwave ($K\uparrow$) and emitted longwave ($L\uparrow$) radiation, net radiation (R_{net}), as well as the sensible heat (H), latent heat (λE), and ground heat (G) fluxes. Our sign convention is that a flux away from the surface is positive, and a flux toward the surface is negative. We first compared the PFT-level (tree and grass PFTs) and grid cell-averaged values of these surface variables at the global scale. For a closer investigation into the temporal differences between the PFTCOL and CTRL simulations, three grid cells were selected, one grid cell from each of the three distinct climate regions: tropical (grid center at 6.13°N, 288.75°E), temperate (35.34°N, 282.5°E), and boreal (66.44°N, 222.5°E). In each of these grid cells, the sum of tree and grass PFT area took up the majority of the grid cell; however, smaller percentages of other PFTs (bare soil or shrubs) did exist in each of these grid cells (Table S1 in the supporting information). These other PFTs are ignored from the PFT-level comparisons but are taken into account in the grid cell-averaged values. For each of these three grid cells, monthly and hourly outputs from the two cases were compared.

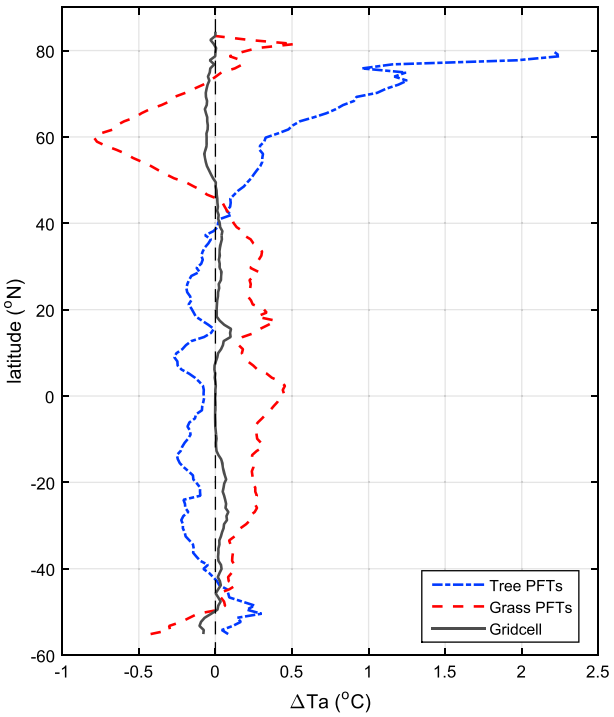

Figure 2. The zonal mean of the difference in 2 m air temperature between the two cases (PFTCOL − CTRL), shown at the grid cell level and PFT-level (PFTs are area-weighted into trees and grasses). Shown as the average of 1991–2010.

Finally, we conducted a comparison of surface air temperature between different land cover types (grass and tree PFTs) within the same grid cell in each simulation. For both the CTRL and PFTCOL cases, the 20 year mean difference in air temperature between grass and tree PFTs (grass air temperature minus tree air temperature, both at the screen height) was calculated. This air temperature difference (ΔT_{GT}) can be thought of as a proxy for a local-scale deforestation signal (i.e., the effect of local-scale deforestation on surface air temperature). While this is not a true deforestation signal, because our offline simulations do not allow the atmosphere to respond to land cover change and do not account for the variations in land cover after deforestation occurs, this method, which substitutes space for time, allows for the comparison of the land surface response of different vegetation types to the same atmospheric conditions. We chose air temperature for this initial comparison of subgrid surface climate because the magnitude and spatial pattern of ΔT_{GT} have been relatively well established in previous observational and modeling studies [e.g., *Davin and de Noblet-Ducoudré*, 2010; *Lee et al.,* 2011; *Zhang et al.,* 2014]. This comparison of air temperature between different land cover types within the same grid cell allows a preliminary assessment of whether the modified subgrid configuration in the PFTCOL simulation improves the subgrid land cover change signal.

In this paper, we first present the global (zonal average) differences in surface variables between the PFTCOL and CTRL simulations. The zonal average is calculated as the arithmetic mean of the difference between tree and grass PFTs across each latitude, including only grid cells that include a fraction of the PFT being averaged. We then discuss the monthly and hourly differences in surface climate variables from the three selected grid cells. The differences are shown in figures in the main text, while the monthly and hourly variations of the actual air temperature and surface energy fluxes are presented in the supporting information (Figures S4–S9). Lastly, we show ΔT_{GT} for both the CTRL and PFTCOL simulations.

3. Results

3.1. Zonal Patterns

Figure 2 presents the zonally averaged difference in 2 m air temperature (ΔT_a) at the PFT-level (grass and tree PFTs) and grid cell-level between the PFTCOL and CTRL simulations (PFTCOL − CTRL). At the grid cell-level, zonal mean ΔT_a is relatively small, ranging from −0.10 K to 0.10 K. At the subgrid or PFT-level, however, ΔT_a is an order of magnitude larger and exhibits distinct latitudinal patterns. Generally, the individual PFT columns produce lower air temperatures over grass PFTs and higher temperatures over tree PFTs in high latitudes, while the reverse is observed in middle to low latitudes (between 40°N and 40°S). The largest differences in T_a between the PFTCOL and CTRL cases for both grass and tree PFTs are observed above 40°N. Above 40°N, the ΔT_a of tree PFTs reaches 2.25 K, while the ΔT_a of grass PFTs reaches −0.79 K. However, it should be noted that the large differences at highest latitudes (>75°N) result from averaging across a low number of grid cells. Global maps of ΔT_a are presented in Figure S1. This warming and cooling pattern for tree and grass PFTs in high latitudes is dominated by changes in air temperature during winter months, resulting from snow cover and albedo changes, as will be discussed in more detail in later sections.

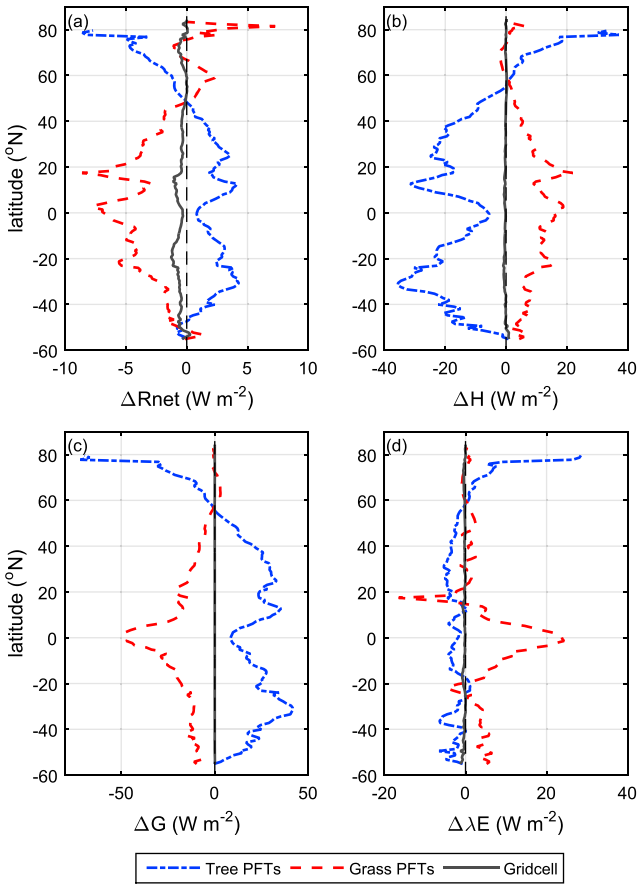

Figure 3. The zonal mean of the differences in (a) net radiation, (b) sensible heat flux, (c) ground heat flux, and (d) latent heat flux between the PFTCOL and CTRL cases (1991–2010).

The configuration of columns, either shared as in the CTRL case or individual as in the PFTCOL case, has a considerable effect on how surface energy is partitioned between radiative, turbulent, and ground heat fluxes at the PFT-level while only minimally affecting the grid cell-averaged values of surface energy fluxes. Figure 3 presents the zonally averaged PFTCOL − CTRL grid cell-level and PFT-level differences in surface energy fluxes: net radiation (ΔR_{net}), sensible heat flux (ΔH), ground heat flux (ΔG), and latent heat flux ($\Delta \lambda E$). Global maps of these data are given in Figure S2. Because CLM4.5 in both the PFTCOL and CTRL cases is forced by the same atmospheric data, changes in net radiation between the two cases are due only to changes in emitted longwave and reflected shortwave radiation from the land surface. The overall zonal patterns in ΔR_{net} for tree and grass PFTs are dominated primarily by changes in emitted longwave radiation. At high latitudes, changes in albedo, and therefore reflected solar radiation, are an important contributor to ΔR_{net}, particularly for grass PFTs. The magnitude of ΔR_{net} is similar for both grass and tree PFTs, although opposite in sign. Across all latitudes, ΔR_{net} for tree PFTs ranges from $-8.6\,W\,m^{-2}$ to $4.3\,W\,m^{-2}$, while ΔR_{net} for grass PFTs ranges from $-8.6\,W\,m^{-2}$ to $7.3\,W\,m^{-2}$. At the grid cell-level, ΔR_{net} is relatively small, ranging from $-1.3\,W\,m^{-2}$ to $0.3\,W\,m^{-2}$.

Changes in the turbulent fluxes are evident at the PFT-level but are relatively small at the grid cell-level. Below 60°N, ΔH for tree PFTs is negative, with the largest decrease ($-36\,W\,m^{-2}$) occurring in midlatitudes. North of 60°N, ΔH is positive for tree PFTs, reaching of $37\,W\,m^{-2}$. The ΔH of grass PFTs is positive (up to $22\,W\,m^{-2}$) over most latitudes, becoming slightly negative at high latitudes. Compared to ΔH at the PFT-level, ΔH at the grid cell-level is quite small (less than $1\,W\,m^{-2}$ in magnitude) over all latitudes. The PFT-level $\Delta \lambda E$ follows a similar pattern to ΔH, with the exception of the tropics, where there was a large increase in λE in the PFTCOL relative to the CTRL case. It was unexpected that ΔH and $\Delta \lambda E$ from each of the two PFT categories did not offset each other. Where ΔH was positive, we expected $\Delta \lambda E$ to be negative, and vice versa, particularly because the magnitude of ΔR_{net} for each of the PFT classes was less than $\pm 10\,W\,m^{-2}$. However, after accounting for ΔG, the surface energy budget for tree and grass PFTs was balanced.

Examining PFT-level ΔG reveals the influence of the shared versus individualized soil columns on the surface energy budget of PFTs and why PFT-level data may be biased in the shared column configuration. The ground heat flux exhibited the largest difference of all surface energy fluxes between the PFTCOL and CTRL cases. Notably, the large ΔG at the PFT level is due to the fact that the annual PFT-level G in the CTRL case is strongly negative or positive, by up to $50\,W\,m^{-2}$ in magnitude at some latitudes, while the annual PFT-level G in the PFTCOL case is approximately zero. For tree PFTs, ΔG ranges from $-71.8\,W\,m^{-2}$ to $41.7\,W\,m^{-2}$, while for grass PFTs, ΔG ranges from $-47.8\,W\,m^{-2}$ to $3.0\,W\,m^{-2}$. The grid cell-averaged ΔG is very small ($\pm 0.1\,W\,m^{-2}$) between the two cases.

Table 1. A Summary of the Annual 2 m Air Temperature (K) and Surface Energy Fluxes (W m^{-2}) for Each of the Three Grid Cells[a]

		Grass PFTs								Tree PFTs							
Grid Location	Case Name	T_a	$K\downarrow$	$K\uparrow$	$L\downarrow$	$L\uparrow$	H	λE	G	T_a	$K\downarrow$	$K\uparrow$	$L\downarrow$	$L\uparrow$	H	λE	G
Boreal (66.44°N, 222.5°E)	PFTCOL	261.8	111.2	41.4	218	266.6	5.7	14.7	0.8	262.3	111.2	11.1	218	274.5	27.7	15.3	0.7
	CTRL	262.5	111.2	37.4	218	271.2	7.6	15.7	-2.6	261.7	111.2	11.2	218	272.2	28.6	17	0.2
	Δ	−0.7	--	4	--	−4.6	−1.9	−1	3.4	0.6	--	−0.1	--	2.3	−0.9	−1.7	0.5
Temperate (35.34°N, 282.5°E)	PFTCOL	288.5	192.7	29.2	337.8	398.4	29.4	73.4	0.06	288.1	192.7	18	337.8	394.3	47.5	70.8	−0.02
	CTRL	288.3	192.7	29.2	337.8	396.4	22.5	68.5	14	288.3	192.7	18	337.8	395.7	55.7	77.6	−16.4
	Δ	0.2	--	0	--	2	6.9	4.9	−13.94	−0.2	--	0	--	−1.4	−8.2	−6.8	16.38
Tropical (6.13°N, 288.75°E)	PFTCOL	300.6	207.3	30.7	429.2	470.8	31.7	103.3	−0.04	299.8	207.3	26.4	429.2	459.3	45.2	105.6	−0.03
	CTRL	300.5	207.3	30.7	429.2	468.4	26.2	96.5	14.7	300.2	207.3	26.4	429.2	463	61.2	117.7	−31.8
	Δ	0.1	--	0	--	2.4	5.5	6.8	−14.74	−0.4	--	0	--	−3.7	−16	−12.1	31.77

[a]The 20 year annual averages for the PFTCOL and CTRL simulations are shown, as well as the difference (Δ) between the two runs (PFTCOL − CTRL).

3.2. Temporal Patterns

Here we compare the PFT-level monthly 2 m air temperature and energy fluxes between the PFTCOL and CTRL cases for each of the three grid cells in the tropical, temperate, and boreal regions. For diurnal differences, we focus on the diurnal patterns of ΔT_a and ΔG for each of the three grid cells. A summary of the annual differences in T_a and surface energy fluxes for each of these three grid cells is presented in Table 1. The seasonality of the monthly atmospheric forcing data for each of these three grid cells is shown in Figure S3.

3.2.1. Seasonal Patterns

Figure 4 presents the monthly differences in 2 m air temperature and surface energy fluxes for tree and grass PFTs between the PFTCOL and CTRL simulations for the tropical grid cell. For 2 m air temperature and the radiative fluxes, the differences between the two cases exhibit little seasonality. The ΔT_a is negative for tree PFTs and positive for grass PFTs over all months, with seasonal variations in the range of only 0.15 to 0.25 K. Across all seasons, PFT-level ΔR_{net} is driven by changes to emitted longwave radiation ($\Delta L\uparrow$). The $\Delta L\uparrow$ for tree and grass PFTs follows ΔT_a: a cooling of tree PFTs in the PFTCOL case results in reduced $L\uparrow$ and thus a higher R_{net}, while the opposite is true for grass PFTs. The ΔR_{net} for tree PFTs peaked at 5.4 W m^{-2}, while ΔR_{net} for grass PFTs reached −4.8 W m^{-2}.

There is some seasonality to the H and λE (Figure S4), due to a dry season from January to March and relatively wetter conditions from April to December. Although the sign of ΔH for both tree and grass PFTs does not change over the year, ΔH is largest in magnitude during the dry season (−31.5 W m^{-2} for tree PFTs and 13.0 W m^{-2} for grass PFTs). In contrast to ΔH, the largest differences in λE for both tree and grass PFTs between the PFTCOL and CTRL simulations are observed during the wet season. The PFTCOL configuration results in a reduction of λE for tree PFTs and an increase in λE for grass PFTs over most of the year (March–December). The largest reduction in λE for tree PFTs between the PFTCOL and CTRL cases occurs in May from 138.1 W m^{-2} in the CTRL case to 118.5 W m^{-2} (Figure S4) in the PFTCOL case. For grass PFTs, the $\Delta\lambda E$ peaked in September at 10.9 W m^{-2}.

In this tropical grid cell, large differences in the ground heat flux are observed between the two cases. In the CTRL case, G is positive (into the soil) year round for grass PFTs (11.3 W m^{-2} to 17.9 W m^{-2}) and negative year round for tree PFTs (−39.0 W m^{-2} to −22.8 W m^{-2}) (Figure S4). In the PFTCOL case, however, the monthly G for tree and grass PFTs ranges from −2.0 W m^{-2} to 2.5 W m^{-2}. Averaging over the entire year, the PFTCOL PFT-level G is nearly zero, while the CTRL case produces annual averages for G of −31.8 W m^{-2} and 14.7 W m^{-2} for tree and grass PFTs, respectively (Table 1). The largest differences are observed in April, with ΔG reaching 38.4 W m^{-2} for tree PFTs and −17.9 W m^{-2} for grass PFTs.

For the temperate grid cell, there is a distinct seasonality to the monthly differences between the PFTCOL and CTRL cases, with the largest differences in all surface variables occurring during summer months (June-August; Figure 5). The magnitude of the differences tends to follow the seasonality of T_a and surface energy fluxes (Figure S5). The ΔT_a for tree PFTs is negative across all months, reaching −0.27 K in June, while ΔT_a for grass PFTs is positive for all months except December, peaking at 0.24 K. The seasonal pattern of PFT-level ΔR_{net} is driven primarily by $\Delta L\uparrow$, as at this latitude; snow cover is not yet a significant contributor to R_{net} in winter months.

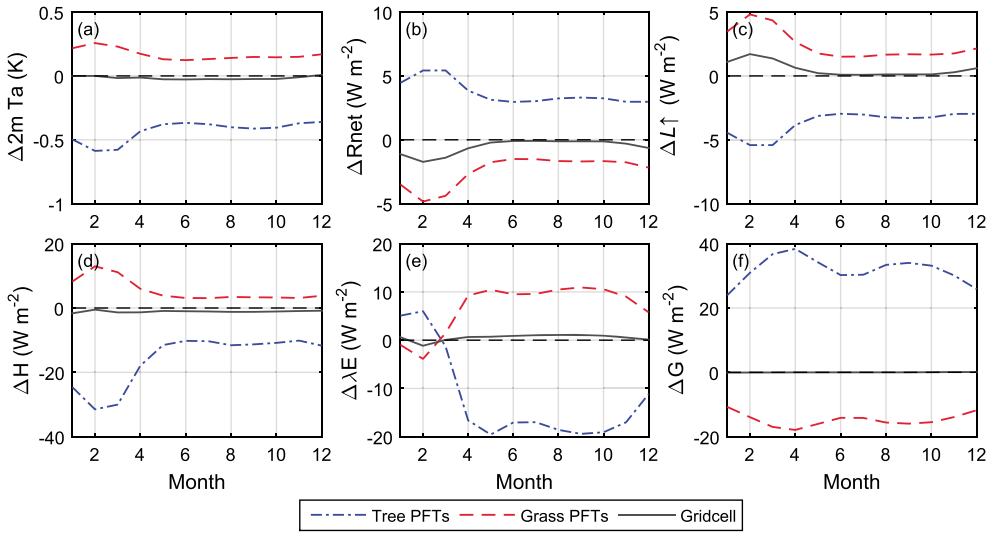

Figure 4. The monthly differences of (a) 2 m air temperature, (b) net radiation, (c) emitted longwave radiation, (d) albedo, (e) sensible heat flux, (f) latent heat flux, and (g) ground heat flux at the tree and grass PFT level and grid cell level for the tropical grid cell (6.13°N, 288.75°E). The monthly differences are averaged over 20 years (1991–2010).

The largest differences in the sensible heat, latent heat, and ground heat fluxes between the PFTCOL and CTRL cases in the temperate grid cell occur during spring and summer months, when fluxes are highest. During summer months, there was a 12 W m^{-2} decrease in H for tree PFTs and a 10 W m^{-2} increase for grass PFTs in the PFTCOL case relative to the CTRL case (Figure S5). The $\Delta\lambda E$ at the PFT level is in the range of ±1 W m^{-2} to 11 W m^{-2} for both grass and tree PFTs.

The magnitude of ΔG is nearly double those of ΔH and $\Delta\lambda E$ for both tree and grass PFTs. In the CTRL case, the ground heat flux for tree PFTs is negative over the entire year, while G for grass PFTs is positive nine months out of the year (Figure S5), resulting in annual averages of −16.4 W m^{-2} and 14.0 W m^{-2} (Table 1). In contrast, G for each of the PFTs in the PFTCOL case exhibits a seasonal cycle (positive flux during summer months and negative flux during winter months) which averages out on an annual basis to be approximately zero (Figure S5 and Table 1). Because of these differences in the seasonality of G between the PFTCOL and CTRL cases, ΔG is large, reaching 25.0 W m^{-2} for grass PFTs and −21.2 W m^{-2} for tree PFTs during the summer.

In the boreal grid cell, the seasonal patterns of air temperature and surface energy fluxes show two interesting differences compared to the temperate and tropical grid cells (Figure 6). First, the largest changes in air temperature between the PFTCOL and CTRL cases occur during winter months. In the PFTCOL case, tree PFTs become cooler during the spring/summer and warmer during the fall and winter, with ΔT_a reaching 1.50 K in February. The ΔT_a for grass PFTs displays an opposite seasonal pattern of the tree PFTs, with slightly positive values from May to August and negative values during the colder months of the year. The warming of grass PFTs during summer months in the PFTCOL case is minimal, but the cooling is substantial, with ΔT_a reaching −1.79 K in April.

Second, $\Delta K\uparrow$ becomes important to ΔR_{net} in the boreal grid cell. In particular, $\Delta K\uparrow$ of grass PFTs contributes significantly to ΔR_{net} in late spring. The ΔR_{net} for grass PFTs in May is −29.0 W m^{-2}, resulting from a $\Delta L\uparrow$ of −13.0 W m^{-2} and a $\Delta K\uparrow$ of 42.0 W m^{-2} (Figure S6). To put $\Delta K\uparrow$ in context with incoming shortwave radiation, the albedo of grass PFTs in May increased from 0.16 in the CTRL case to 0.27 in the PFTCOL case. Dividing the shared soil column into separate columns for each PFT affects snow depth and subsequently the vertical burial of vegetation by snow, since snow is a column-level variable. In the month of May in particular, deeper snow reduces the exposed leaf area index (LAI) of grass PFTs by 0.38 m^2 m^{-2}, while there is no change in the exposed LAI of tree PFTs.

A seasonal cycle exists for ΔH, $\Delta\lambda E$, and ΔG for tree and grass PFTs in the boreal grid cell. Again, the largest change to the surface energy budget between the two cases is to the ground heat flux, with monthly ΔG for tree PFTs and grass PFTs reaching 24.3 W m^{-2} and 20.0 W m^{-2}, respectively. On an annual basis, however, ΔG is relatively small compared to the other two grid cells: 3.4 W m^{-2} for grass PFTs and 0.5 W m^{-2} for tree PFTs (Table 1).

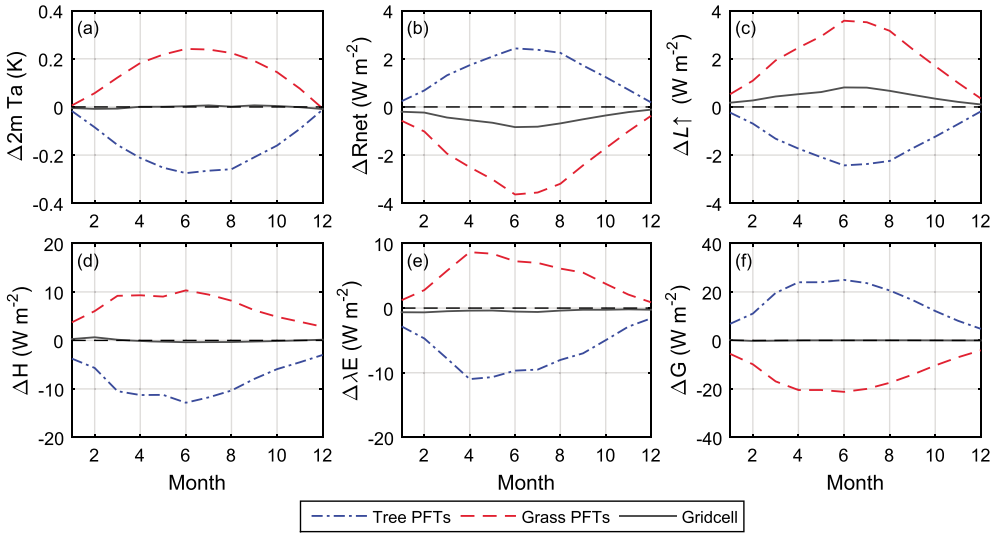

Figure 5. The same as Figure 4 except for the temperate grid cell (35.34°N, 282.5°E).

3.2.2. Diurnal Patterns

We focus on the diurnal patterns of ΔT_a and ΔG for each of the tropical, temperate, and boreal grid cells (Figures 7 and 8). The diurnal patterns and differences of these and other surface variables are given in the supporting information Figures S7–S9. The diurnal ΔT_a patterns are similar in the tropical and temperate grid cells, although they are more pronounced in the tropical grid cell (Figure 7). In the tropical grid cell, ΔT_a for tree PFTs is always negative, reaching -0.82 K during the night, while ΔT_a for grass PFTs is always positive, peaking at 0.25 K overnight. For the temperate grid cell, ΔT_a ranges from -0.40 K for tree PFTs and 0.32 K for grass PFTs. In the boreal grid cell, the hourly ΔT_a is always positive for tree PFTs (up to 0.73 K) and always negative for grass PFTs (up to -0.87 K).

The largest ΔG occurs during midday, when fluxes are the highest (Figure 8). The magnitude of ΔG overshadows those of the other surface energy fluxes, approximately double ΔH and $\Delta \lambda E$ and nearly 10 times larger than ΔR_{net} (Figures S7–S9). In all three grid cells, midday G for tree PFTs is higher in the PFTCOL case relative to the CTRL case, while midday G for grass PFTs is reduced. For tree PFTs, midday ΔG peaks at 98.1 W m^{-2}, 49.9 W m^{-2}, and 12.4 W m^{-2} for the tropical, temperate, and boreal grid cells, respectively. For grass PFTs, midday ΔG reaches -39.3 W m^{-2}, -44.8 W m^{-2}, and -2.9 W m^{-2}.

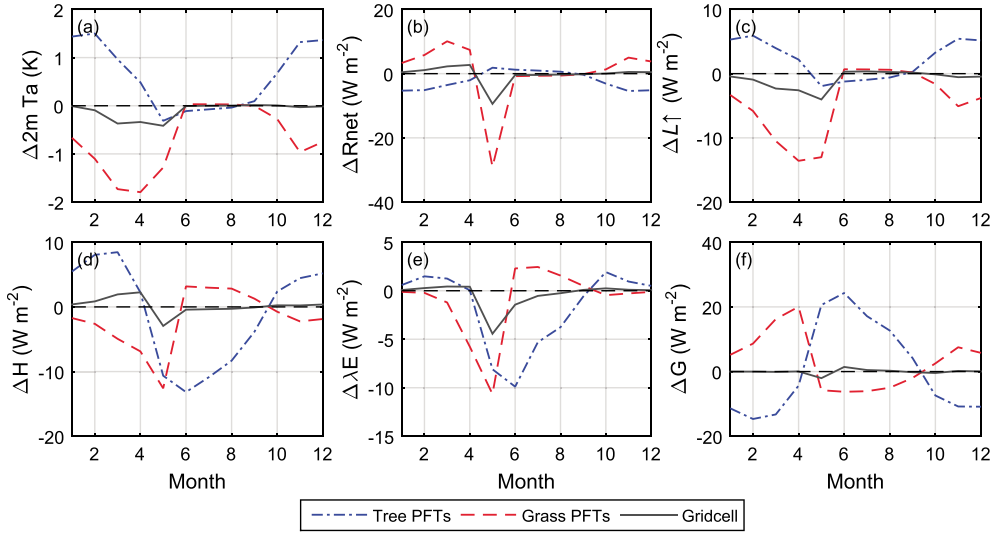

Figure 6. The same as Figure 4 except for the boreal grid cell (66.44°N, 222.5°E).

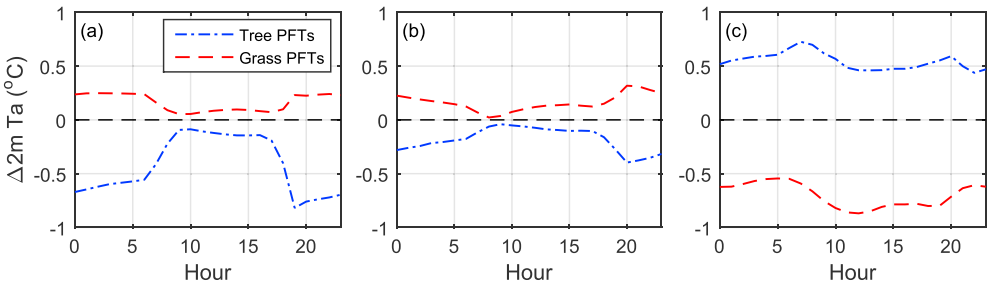

Figure 7. The hourly difference in 2 m air temperature for tree and grass PFTs for the (a) tropical, (b) temperate, and (c) boreal grid cells. The hourly differences are averaged over a single year (2010).

3.3. Subgrid Land Cover Comparison

Figure 9 presents the 20 year average (1991–2010) of the 2 m air temperature difference (ΔT_{GT}) between grass and tree PFTs within each grid cell for the CTRL and PFTCOL simulations. As previously stated, the ΔT_{GT} can be thought of as the effect of local-scale deforestation on surface air temperature. The PFTCOL simulation produces a latitudinal pattern of ΔT_{GT}, with a subgrid cooling of more than 1.5 K in boreal regions and an average subgrid warming in the tropics of approximately 0.6 K. The CTRL simulation produces a spatial pattern of ΔT_{GT} that is nearly opposite to that of the PFTCOL simulation. In the CTRL case, "deforestation" produces the largest warming in high latitudes, with regions of mild cooling scattered across the globe.

4. Discussion

4.1. Soil Column Effect on Subgrid Temperature

Land models typically produce a great amount of subgrid information. The utility of PFT-level data in CLM and possibly other land models is hindered by the implicit transfer of energy through the shared soil column and thus the inability to completely separate a single PFT from the others. By modifying the land surface configuration of CLM in such a way so that each PFT within the vegetated land unit was assigned its own soil column, we showed that each PFT is isolated from the others, allowing for analysis at the PFT-level.

The ΔT_{GT} results from the PFTCOL simulation differ substantially from the CTRL simulation but agree closely with previous studies in both magnitude and latitudinal pattern. The PFTCOL results are in agreement with the observational studies of *Lee et al.* [2011] and *Zhang et al.* [2014] who compared surface air temperature using site pairs of measurements over forests and open lands and found that the magnitude of cooling in high latitudes was higher than the magnitude of warming in low latitudes in both the Americas and Asia. Additionally, these initial results are in general agreement with the annual subgrid canopy air temperature difference (crop − natural vegetation) calculated by *Malyshev et al.* [2015]. They found that compared with natural vegetation, crops produce a local cooling in high latitudes (above approximately 45°N) and warming in middle to low latitudes. The separate soil columns present a new opportunity to isolate the effects of land cover and land cover change on surface climate in GCM experiments.

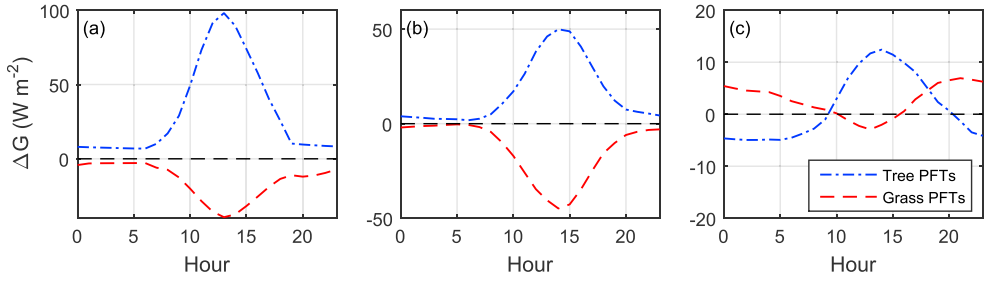

Figure 8. The hourly difference in the ground heat flux for tree and grass PFTs for the (a) tropical, (b) temperate, and (c) boreal grid cells. The hourly differences are averaged over a single year (2010).

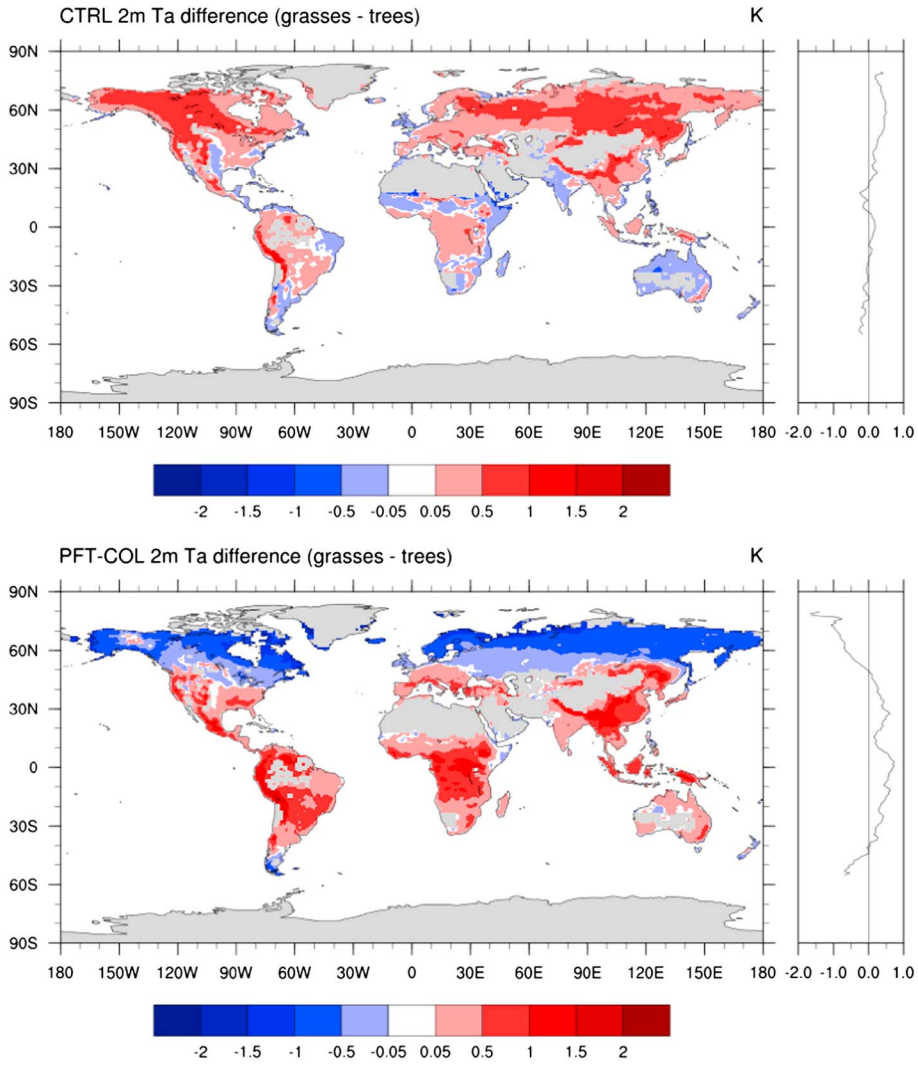

Figure 9. The 20 year (1991–2010) difference in 2 m air temperature (grass PFTs − tree PFTs) for (top) the CTRL case and (bottom) the PFTCOL case. Zonal averages of ΔT_{GT} for each case are shown to the right of the maps.

4.2. Soil Column Effect on PFT Surface Energy Balance

We found that soil column configuration influenced net radiation, turbulent fluxes, and the ground heat flux at the PFT-level, and the difference between the PFTCOL and CTRL simulations increased as the grid cell fraction of the PFT decreased (Figure S10). With regard to the surface energy budget, the largest difference between the PFTCOL and CTRL simulations was found for the ground heat flux (Table 1). The annual mean *G* at the PFT level in the CTRL case is significantly larger than expected in a relatively unchanging climate. By allowing the grass and tree PFTs to share the same soil column, a substantial amount of heat is entering the soil below the grass and coming out of the soil below the tree PFTs. Because there was little to no change in the column-averaged soil temperature despite these large ground heat fluxes, we infer that heat was being transferred from one PFT to another through the shared soil column. Measurements of horizontal soil temperature gradients in heterogeneous landscapes are needed to understand the magnitude of horizontal ground fluxes between different land cover types. However, the CTRL and PFTCOL configurations cannot answer this question, because neither configuration allows for horizontal heat transfer between different PFTs.

The ground heat flux in CLM is calculated as the residual of the surface energy balance equation [*Oleson et al.*, 2013]. Therefore, the nonzero *G* in the CTRL simulation had to have been made up for by smaller or larger PFT-level sensible and latent heat fluxes. The magnitude of changes in these fluxes between the PFTCOL and CTRL cases was significant: In the tropical grid cell, for example, *H* and λE for tree PFTs decreased by

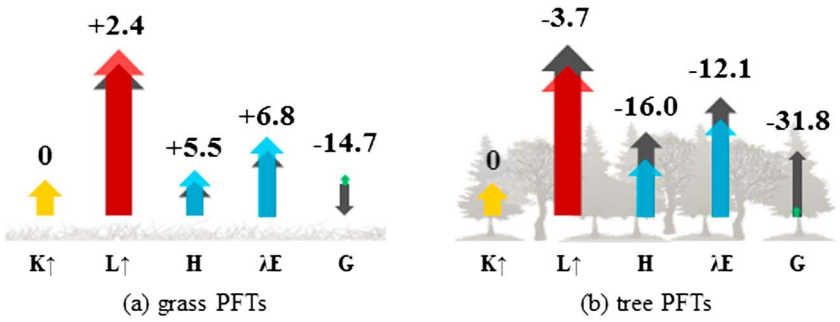

Figure 10. The 20 year annual mean difference (PFTCOL − CTRL) in surface energy fluxes for (a) grass PFTs and (b) tree PFTs in the tropical grid cell. The colored arrows represent fluxes from the PFTCOL case, while grey arrows represent fluxes from the CTRL case. All units are in W m^{-2}.

26% and 10%, respectively, while H and λE for grass PFTs increased by 21% and 7% (Figure 10 and Table 1). We can infer that the turbulent fluxes in the CTRL case are biased at the PFT-level because large negative or positive residual ground heat fluxes are produced. Yet, these biases seem to offset each other, since there are only minimal differences in the grid cell averages. As will be discussed in the following section, this is not to say that the PFTCOL results do not have their own biases. However, we propose that the PFTCOL configuration is useful for diagnosing model biases at their source: the PFT-level.

4.3. Model Evaluation and Validation

Our results indicate that the PFTCOL land surface configuration can also be used for larger-scale evaluation and validation of PFT-level processes. The configuration of the PFTCOL case can be thought of as an expansion of CLM run in single-point mode. Single-point simulations consist of a single point with one PFT on a single column, forced with a prescribed atmospheric data set or flux tower [*Oleson et al.,* 2013]. Often, single-point simulations are used for evaluating specific vegetation types, testing new model schemes, or running CLM over a specific site with observed data [e.g., *Bonan et al.,* 2014; *Chen et al.,* 2015]. Because CLM calculates surface variables at the PFT level, model evaluation at the PFT level may be able to identify potential errors at their source and therefore improve both subgrid and grid cell-averaged outputs. It should be noted, however, that the separate columns increased the computational time of the CLM simulation, with the PFTCOL case costing approximately 11% more than the CTRL case, a relatively minor slowdown when running CLM offline.

The value of this configuration for validation is highlighted through our identification of potential model biases in tropical regions. In the tropics, our PFT-level data show that CLM does not reproduce observed differences in energy partitioning between forested and deforested areas. Comparative flux measurements by *von Randow et al.* [2004] show that the difference in the latent heat flux between forest and pasture site ranges from 21.5 W m^{-2} in the wet season to 44.7 W m^{-2} in the dry season. From our PFTCOL simulation, the difference in λE between grass and forest PFTs was less than 10 W m^{-2} across all seasons (Figure S4). The small contrast in λE between tropical PFTs results in an inaccurate partitioning of the biophysical effects on surface temperature. From flux tower observations, *Lee et al.* [2011] found that deforested tropical sites were nearly 2 K warmer than tropical forests, attributable in large part to changes in the Bowen ratio between the forested and open sites. In paired CLM4.5 simulations by *Chen and Dirmeyer* [2016], however, there was higher ET in the tropics in the deforestation scenario, resulting in a negative contribution of the Bowen ratio effect on surface temperature.

In tropical regions, observations show that forest transpiration is sustained during the dry season and the seasonal change in energy partitioning between H and λE is small [*da Rocha et al.,* 2004; *von Randow et al.,* 2004]. In contrast, observations over deforested areas show a reduced λE during the dry season, accompanied by an increase in H [*von Randow et al.,* 2004]. *Von Randow et al.* [2004] show that the Bowen ratio ($\beta = H/\lambda E$) is relatively constant over a tropical forest across a year, varying between 0.3 and 0.4, while the seasonal β at a nearby pasture site varies from 0.55 during the wet season to 0.77 during the dry season. From the tropical grid cell in this analysis, the annual PFT-level Bowen ratios from the PFTCOL simulation are in better agreement with the measurements of *von Randow et al.* [2004]. Despite improvements in the PFTCOL case, the β of tree PFTs displayed a much larger seasonal change, from 0.33 in the wet season to 0.76 in the dry season,

Table 2. The Root Depth, Bowen Ratio (β), and Soil Water Content for PFTs in the Tropical Grid Cell[a]

			Wet Season (Jul–Sep)					Dry Season (Jan–Mar)				
	Root Depth (m)		β			Soil Water Content (mm)		β			Soil Water Content (mm)	
	PFT #1	PFT #2	PFTCOL	CTRL	Δ	0–2.3 m	2.3–3.8 m	PFTCOL	CTRL	Δ	0–2.3 m	2.3–3.8 m
Grass PFTs	2.3[b]	1.4[c]	0.24	0.23	0.01	833	593	0.58	0.44	0.14	536	521
Tree PFTs	3.8[d]	2.3[e]	0.33	0.37	−0.04	835	589	0.76	1.14	−0.38	566	520

[a]All values are averaged over 20 years (1991–2010) and divided into wet and dry seasons.
[b]C4 grass.
[c]Generic C3 crop.
[d]Broadleaf evergreen tree.
[e]Broadleaf deciduous tree.

than those reported from field observations, showing that the energy partitioning between sensible and latent heat fluxes at the PFT level in CLM4.5 is inconsistent with field observations.

Through the PFT-level analysis, we identified two potential areas of focus for improving PFT-level latent heat flux and energy partitioning in the tropical zone. First, such an improvement may be accomplished through an improved parameterization of below-ground processes. The vertical root distribution affects the rates at which plants extract water from different soil layers for transpiration [*Zeng*, 2001]. The effective rooting depth, defined here as the depth at 99% of the cumulative root fraction, for each of the four PFTs in the tropical grid cell (two grasses and two trees) is given in Table 2. Using the plant-dependent root distribution parameters adopted from *Zeng* [2001], the rooting depths of the C4 grass, C3 crop, broadleaf evergreen trees (BET), and broadleaf deciduous trees (BDT) are 2.3 m, 1.4 m, 3.8 m, and 2.3 m. The similar rooting distributions of tree and grass PFTs are unable to simulate observed differences in soil moisture between these different land cover types. *Von Randow et al.* [2004] found that water storage in the 0–2 m soil layer ranged from approximately 380 mm in the dry season to 800 mm in wet season in the forest and from 420 mm to 700 mm in the pasture, and water storage in the 2.0–3.4 m soil layer in the forest ranged from 200 mm to 500 mm and from 400 mm to 550 mm in the pasture. The large seasonal amplitude of the 2.0–3.4 m layer soil moisture in the forest compared to the minor seasonal variations in the lower soil layer in the pasture indicates larger root uptake from below 2 m in the forest, compared to the pasture. For comparison, little contrast is seen in the modeled soil moisture between grass and tree PFTs (Table 2). From this analysis, extending the rooting system and improving root parameterizations of the tree PFTs may improve the seasonality of energy partitioning of the tree PFTs.

Second, revisions to canopy parameterizations may improve energy partitioning of PFTs in the tropics. The empirical Ball-Berry stomatal conductance model [*Ball et al.,* 1987] is used in CLM4.5 to simulate biotic regulation of ET, but there is some uncertainty as to how to represent stomatal closure as soil moisture declines [*Bonan et al.,* 2014]. Adjusting PFT-dependent photosynthetic parameters that control stomatal resistance has been shown to reduce or offset model errors [*Bonan et al.,* 2011]. Refinement of the canopy model in CLM is another avenue for potential improvements. For example, a multilayer canopy model by *Bonan et al.* [2014] performed better than the CLM Ball-Berry model in flux tower simulations, particularly during times of moisture stress. Additionally, the lack of contrast between the λE of tree and grass PFTs may be due to excessively high ground evaporation and canopy transpiration from grass PFTs [*Chen and Dirmeyer*, 2016]. *Swenson and Lawrence* [2014] have shown that soil evaporation in CLM4.5 is biased high over sparse canopies. Revisions to soil evaporation in CLM should result in further improvements.

4.4. Column Effect on Coupled Simulations and Carbon Balance

Despite large changes at the PFT level between the PFTCOL and CTRL simulations, the grid cell-averaged differences between the two cases were minimal, because the changes in the surface variables for tree PFTs were offset by changes in the other direction for grass PFTs. Therefore, a PFTCOL configuration of CLM4.5 coupled to the atmospheric model will not significantly modify atmospheric processes. However, there is evidence that the representation of the land surface in terrestrial models affects the carbon balance at both the PFT and grid cell levels. *Li and Arora* [2012] compared the carbon balance of a land surface model using both the composite and mosaic approaches, finding that the grid cell-averaged carbon flux differed

between the two approaches by as much as 41% for net primary productivity, 16% for vegetation biomass, and 46% for soil carbon mass. Additionally, *Melton and Arora* [2014] found that land model surface configuration had a significant influence on the modeled response of terrestrial carbon to land cover change, with the composite and mosaic approaches differing by 16% in estimates of the terrestrial carbon sink. This topic has not yet been investigated using CLM; however, as with the physical surface processes, individual columns may prove as a useful tool for model evaluation.

5. Conclusions

We found that the spatial pattern and magnitude of ΔT_{GT} (2 m air temperature difference between grass and tree PFTs) from the PFTCOL simulation agreed closely with previously published studies, with grasses typically exhibiting lower mean annual temperatures in boreal regions and higher temperatures in the tropics than forests. The CTRL case was not able to simulate these same patterns at the subgrid level.

Between the PFTCOL and CTRL cases, there were large PFT-level differences in 2 m air temperature and surface energy fluxes, particularly the ground heat flux (G). As *G* is calculated as the residual of the surface energy budget, we infer that the latent and sensible heat fluxes in the CTRL case were biased either high or low depending on the large negative or positive ground heat flux. The large PFT-level ground heat fluxes in the CTRL case imply a transfer of energy between PFTs through the shared soil column, complicating the interpretation of PFT-level fluxes. This issue does not exist in the PFTCOL configuration, which presents the opportunity to both evaluate the simulation of PFT-level processes and to compare biophysical processes between different vegetation types.

Land models produce a large amount of subgrid information; however, PFT-level data are rarely used in GCM experiments. Here we show that the PFTCOL configuration appears to be promising for evaluation of biophysical land cover change impacts and for assessment of PFT-level representations of fluxes.

Acknowledgments
We would like to acknowledge high-performance computing support from Yellowstone (ark:/85065/d7wd3xhc) provided by NCAR's Computational and Information Systems Laboratory, sponsored by the National Science Foundation. We would also like to acknowledge financial support from Yale University and NCAR's ASP Graduate Visitor Program. The Community Earth System Model is freely available at http://www.cesm.ucar.edu/models/cesm1.2/. The modified code and data used for this analysis are available from authors upon request (natalie.schultz@yale.edu). We thank two anonymous reviewers whose comments helped us improve this paper.

References

Arain, M. A., E. J. Burke, Z.-L. Yang, and W. J. Shuttleworth (1999), Implementing surface parameter aggregation rules in the CCM3 global climate model: Regional responses at the land surface, *Hydrol. Earth Syst. Sci.*, *3*(4), 463–476.

Bala, G., K. Caldeira, M. Wickett, T. J. Phillips, D. B. Lobell, C. Delire, and A. Mirin (2007), Combined climate and carbon-cycle effects of large-scale deforestation, *Proc. Natl. Acad. Sci. U.S.A.*, *104*(16), 6550–6555, doi:10.1073/pnas.0608998104.

Ball, J. T., I. E. Woodrow, and J. A. Berry (1987), A model predicting stomatal conductance and its contribution to the control of photosynthesis under different environmental conditions, in *Progress in Photosynthesis Research*, edited by J. Biggins, pp. 221–224, Kluwer Acad., Dordrecht, Netherlands.

Bonan, G. B. (2008), Forests and climate change: Forcings, feedbacks, and the climate benefits of forests, *Science*, *320*(5882), 1444–1449, doi:10.1126/science.1155121.

Bonan, G. B., P. J. Lawrence, K. W. Oleson, S. Levis, M. Jung, M. Reichstein, D. M. Lawrence, and S. C. Swenson (2011), Improving canopy processes in the Community Land Model version 4 (CLM4) using global flux fields empirically inferred from FLUXNET data, *J. Geophys. Res.*, *116*, G02014, doi:10.1029/2010JG001593.

Bonan, G. B., M. Williams, R. A. Fisher, and K. W. Oleson (2014), Modeling stomatal conductance in the earth system: Linking leaf water-use efficiency and water transport along the soil–plant–atmosphere continuum, *Geosci. Model Dev.*, *7*(5), 2193–2222, doi:10.5194/gmd-7-2193-2014.

Chen, L., and P. A. Dirmeyer (2016), Adapting observationally based metrics of biogeophysical feedbacks from land cover/land use change to climate modeling, *Environ. Res. Lett.*, *11*(3), 034002, doi:10.1088/1748-9326/11/3/034002.

Chen, M., T. J. Griffis, J. M. Baker, J. D. Wood, and K. Xiao (2015), Simulating crop phenology in the Community Land Model and its impact on energy and carbon fluxes, *J. Geophys. Res. Biogeosci.*, *120*, 310–325, doi:10.1002/2014JG002780.

Ciais, P., et al. (2013), Carbon and other biogeochemical cycles, in *Climate Change 2013: The Physical Science Basis. Contribution of Working Group I to the Fifth Assessment Report of the Intergovernmental Panel on Climate Change*, edited by T. F. Stocker et al., pp. 465–570, Cambridge Univ. Press, New York.

da Rocha, H. R., M. L. Goulden, S. D. Miller, M. C. Menton, L. D. V. O. Pinto, H. C. de Freitas, and A. M. e Silva Figueira (2004), Seasonality of water and heat fluxes over a tropical forest in Eastern Amazonia, *Ecol. Appl.*, *14*(4), S22–S32.

Davin, E. L., and N. de Noblet-Ducoudré (2010), Climatic impact of global-scale deforestation: Radiative versus nonradiative processes, *J. Clim.*, *23*(1), 97–112, doi:10.1175/2009jcli3102.1.

Deng, B., S. Liu, W. Xiao, W. Wang, J. Jin, and X. Lee (2013), Evaluation of the CLM4 Lake Model at a large and shallow freshwater lake, *J. Hydrometeorol.*, *14*(2), 636–649, doi:10.1175/jhm-d-12-067.1.

de Noblet-Ducoudré, N., et al. (2012), Determining robust impacts of land-use-induced land cover changes on surface climate over North America and Eurasia: Results from the first set of LUCID experiments, *J. Clim.*, *25*(9), 3261–3281, doi:10.1175/jcli-d-11-00338.1.

Hurrell, J. W., et al. (2013), The Community Earth System Model: A framework for collaborative research, *Bull. Am. Meteorol. Soc.*, *94*(9), 1339–1360, doi:10.1175/bams-d-12-00121.1.

Koster, R. D., and M. J. Suarez (1992), A comparative analysis of two land surface heterogeneity representations, *J. Clim.*, *5*, 1379–1390.

Lawrence, D. M., et al. (2011), Parameterization improvements and functional and structural advances in version 4 of the Community Land Model, *J. Adv. Model. Earth Syst.*, *3*, M03001, doi:10.1029/2011MS000045.

Lawrence, P. J., and T. N. Chase (2007), Representing a new MODIS consistent land surface in the Community Land Model (CLM 3.0), *J. Geophys. Res.*, *112*, G01023, doi:10.1029/2006JG000168.

Lawrence, P. J., and T. N. Chase (2010), Investigating the climate impacts of global land cover change in the community climate system model, *Int. J. Climatol.*, *30*(13), 2066–2087, doi:10.1002/joc.2061.

Lee, X., et al. (2011), Observed increase in local cooling effect of deforestation at higher latitudes, *Nature*, *479*(7373), 384–387, doi:10.1038/nature10588.

Li, R., and V. K. Arora (2012), Effect of mosaic representation of vegetation in land surface schemes on simulated energy and carbon balances, *Biogeosciences*, *9*(1), 593–605, doi:10.5194/bg-9-593-2012.

Mahmood, R., et al. (2014), Land cover changes and their biogeophysical effects on climate, *Int. J. Climatol.*, *34*, 929–953.

Malyshev, S., E. Shevliakova, R. J. Stouffer, and S. W. Pacala (2015), Contrasting local versus regional effects of land-use-change-induced heterogeneity on historical climate: Analysis with the GFDL Earth System Model, *J. Clim.*, *28*(13), 5448–5469, doi:10.1175/jcli-d-14-00586.1.

Melton, J. R., and V. K. Arora (2014), Sub-grid scale representation of vegetation in global land surface schemes: Implications for estimation of the terrestrial carbon sink, *Biogeosciences*, *11*(4), 1021–1036, doi:10.5194/bg-11-1021-2014.

Molod, A. (2002), A global assessment of the mosaic approach to modeling land surface heterogeneity, *J. Geophys. Res.*, *107*(D14), 4217, doi:10.1029/2001JD000588.

Myneni, R. B., et al. (2002), Global products of vegetation leaf area and fraction absorbed PAR from year one of MODIS data, *Remote Sens. Environ.*, *83*, 214–231.

Oleson, K. W., et al. (2013), Technical description of version 4.5 of the Community Land Model (CLM), Rep., Natl. Cent. for Atmos. Res.

Pielke, R. A., R. Avissar, M. Raupach, A. J. Dolman, X. Zeng, and A. S. Denning (1998), Interactions between the atmosphere and terrestrial ecosystems: Influence on weather and climate, *Global Change Biol.*, *4*, 461–475.

Pielke, R. A., et al. (2011), Land use/land cover changes and climate: Modeling analysis and observational evidence, *Wiley Interdiscip. Rev. Clim. Change*, *2*(6), 828–850, doi:10.1002/wcc.144.

Pitman, A. J., et al. (2009), Uncertainties in climate responses to past land cover change: First results from the LUCID intercomparison study, *Geophys. Res. Lett.*, *36*, L14814, doi:10.1029/2009GL039076.

Subin, Z. M., L. N. Murphy, F. Li, C. Bonfils, and W. J. Riley (2012), Boreal lakes moderate seasonal and diurnal temperature variation and perturb atmospheric circulation: Analyses in the Community Earth System Model 1 (CESM1), *Tellus, Ser. A*, *64*, 15639, doi:10.3402/tellusa.v64i0.15639.

Swenson, S. C., and D. M. Lawrence (2014), Assessing a dry surface layer-based soil resistance parameterization for the Community Land Model using GRACE and FLUXNET-MTE data, *J. Geophys. Res. Atmos.*, *119*, 10,299–10,312, doi:10.1002/2014JD022314.

Viovy, N. (2011), CRUNCEP dataset. [Available at http://dods.extra.cea.fr/store/p529viov/cruncep/V4_1901_2011/].

von Randow, C., et al. (2004), Comparative measurements and seasonal variations in energy and carbon exchange over forest and pasture in South West Amazonia, *Theor. Appl. Climatol.*, *78*(1-3), 5–26, doi:10.1007/s00704-004-0041-z.

Zeng, X. (2001), Global vegetation root distribution for land modeling, *J. Hydrometeorol.*, *2*, 525–530.

Zhang, M., et al. (2014), Response of surface air temperature to small-scale land clearing across latitudes, *Environ. Res. Lett.*, *9*(3), 034002, doi:10.1088/1748-9326/9/3/034002.

Zhao, L., X. Lee, R. B. Smith, and K. Oleson (2014), Strong contributions of local background climate to urban heat islands, *Nature*, *511*(7508), 216–219, doi:10.1038/nature13462.